Journal of Alloys and Compounds 509 (2011) 7283–7289

Contents lists available at ScienceDirect

Journal of Alloys and Compounds

journal homepage: www.elsevier.com/locate/jallcom

Nonlinear saturable absorption of the sodium borosilicate glass containing Bi_2S_3 nanocrystals using *Z*-scan technique

Xinyu Yang[a,b], Weidong Xiang[a,b,*], Haijun Zhao[a], Haitao Liu[a], Xiyan Zhang[b], Xiaojuan Liang[a]

[a] College of Chemistry and Materials Engineering, Wenzhou University, Wenzhou 325035, China
[b] College of Materials Science and Engineering, Changchun University of Science and Technology, Changchun 325035, China

ARTICLE INFO

Article history:
Received 8 March 2011
Received in revised form 10 April 2011
Accepted 13 April 2011
Available online 21 April 2011

Keywords:
Semiconductors
Optical materials
Sol–gel processes
Microstructure
Optical properties

ABSTRACT

The sodium borosilicate glass containing Bi_2S_3 nanocrystals is prepared by employing both sol–gel and atmosphere control methods. The third-order nonlinear optical absorption of the glass is investigated in detail using the open-aperture *Z*-scan technique at the wavelength of 770 nm with a pulse width of 200 fs. The results show that the transformation from saturable absorption to reverse saturable absorption in the glass is observed with the increase of the input light intensity of the laser used. The mechanism of the third-order nonlinear optical absorption is discussed preliminarily in the glass. Meanwhile, XRD, XPS, TEM, (S)TEM, EDAX, HRTEM, and SAED are used to characterize the microstructures of the glass.

1. Introduction

Nonlinear absorption is a phenomenon defined as a reduction or increase of the absorption coefficient with the increase of the input light intensity. Nonlinear absorption processes contain saturable absorption (SA), reverse saturable absorption (RSA), two-photon absorption (TPA), and multi-photon absorption (MPA). In particular, materials with saturable absorption (SA) and reverse saturable absorption (RSA) have received a great deal of attention in recent years for a variety of applications such as Q-switching mode-locking, upconversion lasing, and optical limiting, etc. [1–6]. Physically, saturable absorption (SA) indicates that the optical transmittance of materials increases with the input light intensity. It occurs when the ground-state absorption cross section is larger than the one of the excited state, whereas reverse saturable absorption (RSA) indicates that the optical transmittance of materials decreases with the input light intensity. It occurs when the absorption cross section of the excited state is larger than the one of the ground state.

Z-scan technique is a simple, quick, and efficient method to measure the third-order optical nonlinearities of materials. Generally, the open-aperture *Z*-scan model is employed to measure the nonlinear optical absorption of materials. Under such circumstances the normalized transmittance curve exhibits a completely symmetric shape about the waist ($z = 0$). At present, the open-aperture *Z*-scan model is widely used for the nonlinear optical absorption of materials [7–11]. In particular, some studies revealed that many materials exhibit more than one kind of nonlinear optical absorption simultaneously with the change in the input light intensity. Typically, Neo et al. [12] reported on the nonlinear optical absorption in PbS quantum dots changed from SA to RSA with the particle size or intensity. Gurudas et al. [13] found that the SA and RSA coexisted in silver nanodots at 532 nm using picosecond laser pulses. Elim et al. [14] observed the phenomenon of SA and RSA at longitudinal surface plasmon resonance in gold nanorods, and the conversion can occur with the change of excitation irradiances. Qu et al. [15] studied on the optical nonlinear absorption and optical limiting in gold-precipitated glasses induced by a femtosecond laser, and the transformation from SA to RSA was observed in the glasses. Gao et al. [16] explained the transformation from SA to RSA using the phenomenological model of the combination of SA and TPA, and they estimated the saturable intensity and the nonlinear optical absorption coefficient by simulating the experimental curves. Thus it is seen that the nonlinear optical absorption of materials has become the focus of research these years.

As well known, semiconductor materials have attracted increasing interest recently in nonlinear optics [17–20], in which many attentions are focused on the optical nonlinear properties of chalcogenide semiconductor materials [21–25]. Bi_2S_3, as an important semiconductor material with a direct band gap of 1.3 eV, is

* Corresponding author at: College of Chemistry and Materials Engineering, Wenzhou University, Wenzhou 325035, China. Tel.: +86 577 86689640; fax: +86 577 86689644.
E-mail address: weidongxiang@yahoo.com.cn (W. Xiang).

0925-8388/$ – see front matter © 2011 Elsevier B.V. All rights reserved.
doi:10.1016/j.jallcom.2011.04.078

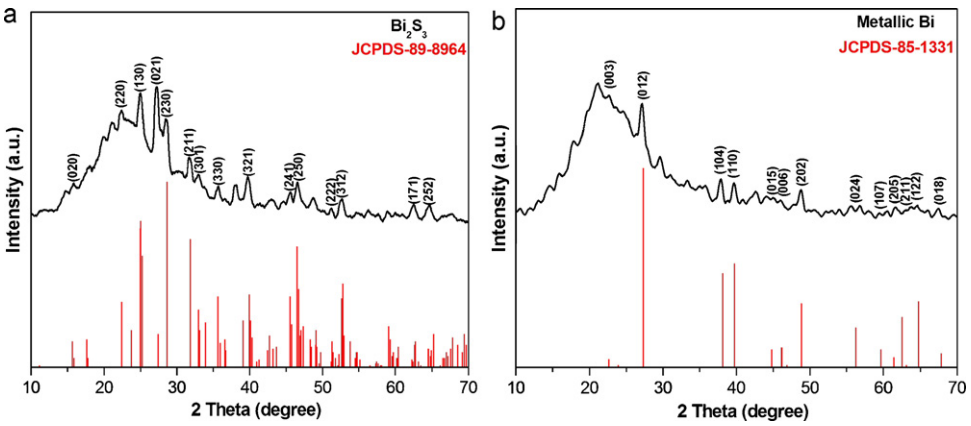

Fig. 1. XRD patterns: (a) $O_2 + H_2 + H_2S$/600 °C and (b) $O_2 + H_2$/450 °C. The JCPDS patterns of Bi_2S_3 and metallic Bi are also shown.

widely studied because of its excellent properties such as photoconductivity, photosensitivity, and thermoelectric effect [26–29]. Recently, research efforts have been directed towards the synthesis of nanometer-sized Bi_2S_3 crystalline materials with the different morphologies (wire [30], tube [31], rod [32], ribbons [33], belt [34], flowers [35], sheaf [36], etc.) because of its unique optical, magnetic, and catalytic properties arising from the quantum size effects. However, few literatures report on the third-order optical nonlinear properties of Bi_2S_3 nanomaterials using *Z*-scan technique to date [37]. In particular, Bi_2S_3 will have the opportunity to achieve strong quantum size effects due to its large Bohr radius [38]. It will greatly promote the development of Bi_2S_3 nanomaterials in nonlinear optics. Moreover, Bi_2S_3 exhibits a quite strong absorption intensity around 400–1000 nm [39], which could contribute to the enhancement of the nonlinear optical absorption. Thus we develop a facile method to realize the preparation of the sodium borosilicate glass containing Bi_2S_3 nanocrystals, and microstructures of the glass are characterized in detail by a variety of techniques. Furthermore, the third-order optical nonlinear absorption of the glass is measured by the open-aperture *Z*-scan model. We initially explore the interplay between saturable absorption (SA) and reverse saturable absorption (RSA) in the *Z*-scan traces under the different input light intensity of laser used, and the third-order nonlinear optical absorption coefficients of the glass are also calculated by the open-aperture *Z*-scan theory.

2. Experimental

The sodium borosilicate glass containing Bi_2S_3 nanocrystals was prepared by employing both sol–gel and atmosphere control methods. The weight composition of the sodium borosilicate glass matrix was $5.74Na_2O$–$21.38B_2O_3$–$72.88SiO_2$ (in wt%). The preparation procedures were as follows: firstly, SiO_2 component was obtained by hydrolysis of tetraethoxysilane (TEOS) in the mixed solution of anhydrous ethanol (EtOH), deionized water (H_2O), and hydrochloric acid (HCl) (pH = 2). Secondly, B_2O_3 and Na_2O were obtained by dissolving boric acid (H_3BO_3) and metallic sodium (Na) in 2-methoxyethanol ($CH_3OCH_2CH_2OH$) and anhydrous ethanol (EtOH), respectively. (Attention please: metallic Na should be slowly added to anhydrous ethanol to prevent the violent reaction.) Here two solutions containing B_2O_3 and Na_2O were added to the solution containing SiO_2 successively. After the mixed solution was stirred for 1 h at room temperature, a methanol (CH_3OH) solution containing 5 wt% of bismuth nitrate [$Bi(NO_3)_3{\cdot}5H_2O$] was added to above mixed solution to form Bi_2S_3 nanocrystals. So the theoretical content of Bi_2S_3 was about 3.77 wt% in the glass matrix [$Bi(NO_3)_3{\cdot}5H_2O$:Bi_2S_3 molar ratio at 1:2], and the theoretical weight ratio of Bi:S:Si:Na, as the major elements in the glass, was about 3.06:0.71:34.01:4.26. Subsequently, the mixed solution was dried at 80 °C for three weeks to form the stiff gel. Finally the stiff gel was heated in different atmosphere by the following steps: firstly, the stiff gel was heated in oxygen (O_2) atmosphere at a rate of 10 °C/h up to 450 °C, and kept 10 h at this temperature to remove organic substance and decompose bismuth nitrate. The loose and porous aerogel will form due to organic substance removed. Secondly, the aerogel is exposed to dry hydrogen (H_2) atmosphere to form metallic Bi at 450 °C for 10 h. Subsequently, hydrogen (H_2) atmosphere was replaced by hydrogen sulfide (H_2S) atmosphere, and the areogel was further heated in hydrogen sulfide (H_2S) atmosphere at 450 °C for 10 h to form Bi_2S_3 nanocrystals. At last, the aerogel was heated in nitrogen (N_2) atmosphere at a rate of 10 °C/h up to 600 °C and kept 10 h at this temperature. The sodium borosilicate glass containing Bi_2S_3 nanocrystals is obtained. The as-obtained glass were cut and polished to a thickness of 0.5 mm for various measurements.

The crystalline structure of these nanoparticles doped in the glass was performed on a Germany Bruker X-ray diffractrometer (40 kV, 20 mA) using Cu Kα radiation (λ = 0.15418 nm) at a scan rate of 0.02°/s in the range 10–70°. The chemical structure and electronic state of the glass were measured by AXIS ULTRA DLD X-ray photoelectron spectrometer (XPS), using monochrome Al Kα as the excitation source. Transmission electron microscopy (TEM), high-resolution TEM (HRTEM), and selected-area electron diffraction (SAED) were recorded on a FEI Tecnai F20 transmission electron microscope operating at 200 kV for the morphology and the crystalline structure of these nanoparticles in the glass. Energy dispersive X-ray (EDX) analysis was carried out on an OXFORD INCA instrument attached to the field emission scanning electron microscope in the scanning range of 0–20 kV to find out the chemical composition. Optical absorption spectrum was measured by JASCO v-570 spectrometer in the range of 350–1500 nm at room temperature. The third-order optical nonlinearities of the glass were measured by *Z*-scan technique. The laser pulses used were generated by a mode-locked Ti:sapphire (Coherent Mira900-D) laser, operating at a repetition rate of 76 MHz with the pulse duration of 200 fs and a wavelength of 770 nm.

3. Results and discussion

3.1. Microstructural characterization

Fig. 1 represents the XRD patterns of the glass. Fig. 1(a) shows that the glass is heat-treated consecutively by oxygen (O_2), hydrogen (H_2), and hydrogen sulfide (H_2S) atmospheres at 600 °C. The joint Committee on Powder Diffraction Standards (JCPDS) pattern of Bi_2S_3 is shown for comparison. It is clear that the diffraction peaks attributed to Bi_2S_3 are observed, which are arranged for orthorhombic crystal system. The result indicates that Bi_2S_3 crystalline structure have formed in the glass. Fig. 1(b) shows that the glass is only heat-treated by oxygen (O_2) and hydrogen (H_2) atmospheres at 450 °C. The joint Committee on Powder Diffraction Standards (JCPDS) pattern of metallic Bi is shown for comparison. The diffraction peaks attributed to metallic Bi are observed. The result indicates that the formation of metallic Bi crystalline structure is a key step towards Bi_2S_3 crystalline structure in the glass. These findings show that using both sol–gel and atmosphere control methods are highly effective for preparation of the sodium borosilicate glass containing Bi_2S_3 crystals.

Furthermore, X-ray photoelectron spectrum (XPS) and transmission electron microscopy (TEM) are employed to characterize the electronic state, morphology, composition, and crystalline structure of the glass. Fig. 2 represents the high-resolution XPS spectra taken for Bi 4f and S 2s regions. In order to analyze the electronic states in more detail, the curve-fitting method is used to study Bi 4f and S 2s cores. Fig. 2(a) represents the high-resolution Bi 4f core spectrum. The three strong peaks for A1, A2, and C at 158.4 eV, 163.7 eV, and 154.7 eV are assigned for Bi $4f_{7/2}$, Bi

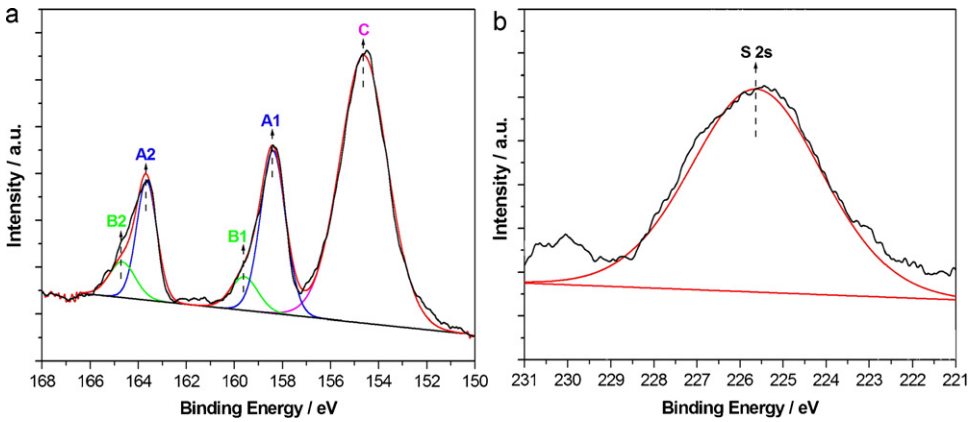

Fig. 2. XPS spectra: (a) high-resolution Bi 4f core and (b) high-resolution S 2s core.

$4f_{5/2}$, and Si 2s cores, respectively. Fig. 2(b) represents the high-resolution S 2s core spectrum. The only one strong peak at 225.6 eV is assigned for S 2s core. The peak positions for Bi 4f and S 2s cores agree well with those reported in the literatures [40,41]. The results indicate that Bi_2S_3 crystalline structure have formed in the glass, which is consistent with XRD analysis. However, the two weak peaks for B1 and B2 at 159.6 eV and 164.7 eV are also observed simultaneously in Fig. 2(a), which should also be assigned for Bi $4f_{7/2}$ and Bi $4f_{5/2}$, respectively. The presence of the two weak peaks is derived from oxidation at the surface of Bi_2S_3 crystals in the air.

Fig. 3 represents the TEM analysis of the glass. Fig. 3(a) represents a typical TEM image of the glass. Obviously, some black nanoparticles having regular spherical in shape are mounted uniformly in the glass, and the diameters of these spherical nanoparticles range from several to over twenty nanometers. The more information of these nanoparticles is further determined by the scanning transmission electron microscopy [(S)TEM]. The (S)TEM is usually used to obtain spatially resolved chemical information about the nanocrystals [42–44]. As heavier elements scatter electrons more effectively, they appear brighter in (S)TEM images. Thus the homogeneous metal sulfide nanocrystals should appear uniformly bright. Fig. 3(b) shows that the bright white spherical nanoparticles with the diameters ranging from several to over twenty nanometers are observed, and the bright white nanoparticles are uniform in intensity. The results indicate that these nanoparticles are likely Bi_2S_3 nanocrystals in our experiment. EDX, HRTEM, and SAED analysis are further employed to analyze the chemical composition and crystalline structure of the nanocrystals glass. Fig. 3(c) represents the EDX spectrum of the glass. It is clear that Bi and S elements, as the composition of nanocrystals, present in EDX spectrum, and Si, O, and Na elements, as the composition of the glass matrix are also observed. However, the peaks of Bi and S elements are weak due to the influence of the strong peaks of Si, O, and Na elements in EDX spectrum. The inset located at red dashed line right in Fig. 3(c) can obviously observe the peaks of Bi and S elements in the absence of Si, O and Na elements. Meanwhile, the EDX spectrum also reveals that the actual weight ratio of Bi:S:Si:Na is about 3.01:0.68:33.96:4.25, which basically agrees well with the theoretical content. The relative error may be caused due to evaporation losses in heat-treatment course. Fig. 3(d) and (e) represents the HRTEM and SAED images of these nanoparticles, respectively. The inset shown in red square frame is a partial enlarged detail for the obvious observation of the lattice fringe, as shown in Fig. 3(d). It is clear that the lattice fringe spacing is equal to 0.360 nm correspond to the (1 1 1) plane of Bi_2S_3 in an orthorhombic crystal system (JCPDS 89-8964), and some light diffraction spots are characteristic crystal planes of Bi_2S_3 in a orthorhombic crystal system (JCPDS 89-8964) by means of measuring the distances d between diffraction spots and base point, as shown in Fig. 3(e). HRTEM and SAED analysis further confirm that these nanoparticles mounted in the glass matrix should be Bi_2S_3 nanocrystals.

3.2. Optical absorption analysis

Fig. 4 represents the optical absorption spectrum of the glass from 350 to 1500 nm. No obvious absorption peaks are observed, that is, the glass has no observable absorption at a laser frequency of 770 nm. The inset in Fig. 4 shows that plot of $[\alpha(h\nu)]^2$ vs. photon energy ($h\nu$) for the glass. According to the well-known Tauc law [45], E_g can be obtained with the following Eq. (1):

$$\alpha(h\nu) = A(h\nu - E_g)^m \quad (1)$$

In the above equation, $\alpha(h\nu)$ is the absorption coefficient, E_g is the band gap energy, A is a constant. Bi_2S_3 is a semiconductor with a direct band gap, and the exponent m should be 1/2. Therefore, the band gap energy is determined by extrapolating the linear portion of the curve to the energy axis. The optical band gap is found to be 1.6733 eV while the reported values of the optical band gap of Bi_2S_3 for bulk material is 1.3 eV. The red shift of the optical band gap in inset displays the quantum size effects, which will contribute to the enhancement of the nonlinear optical properties of the glass.

3.3. Third-order nonlinear optical absorption analysis

The third-order optical nonlinear absorption of the glass is measured by the open-aperture Z-scan technique at 770 nm. No scattering signal is observed in the process of the open-aperture Z-scan measurement. Fig. 5 represents the normalized transmittance curves of the glass at the input light intensities of 0.78×10^{13} W/m^2 and 1.11×10^{13} W/m^2, respectively. At the lower input light intensity of 0.78×10^{13} W/m^2, the normalized transmittance curve, as shown in red fitting curve, exhibits a symmetrical peak with respect to the focus ($z = 0$), indicating that saturable absorption (SA) occurs in the glass by now. With the input light intensity increased to 1.11×10^{13} W/m^2, the normalized transmittance curve, as shown in blue fitting curve, exhibits a symmetrical valley with respect to the focus ($z = 0$), indicating that reverse saturable absorption (RSA) occurs in the glass. The results indicate that the transformation from SA to RSA occurs in the glass with the increase of the input light intensity.

The third-order optical nonlinear absorption coefficient β of the glass is calculated at the two input light intensities by the following Eq. (2):

$$\Delta\psi = \frac{\beta I_0 L_{\text{eff}}}{2} \quad (2)$$

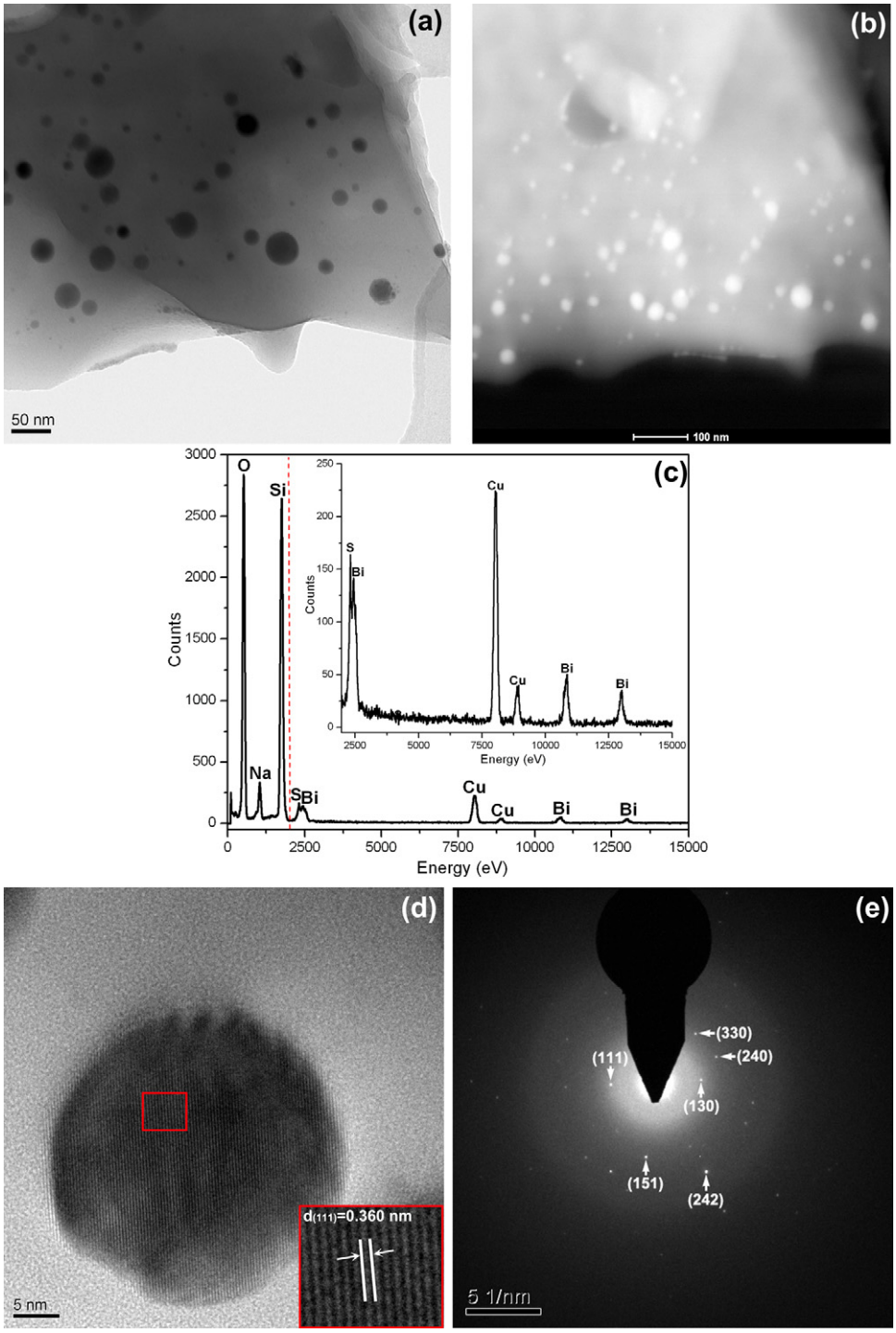

Fig. 3. TEM analysis: (a) morphology image, (b) (S)TEM image, (c) EDX spectrum, (d) HRTEM image and (e) SAED image.

where $\Delta\psi$ are the nonlinear phase shifts due to the third-order optical nonlinear absorption. I_0 is the on-axis irradiance of the laser beam used at the focus ($z=0$), $I_0 = 2P/[\pi\omega_0^2(1-e^{-2})]$ defined as the power density within the glass, and ω_0 is the beam waist radius at the focus ($z=0$). L_{eff} is the effective length of the glass, $L_{\text{eff}} = [1-\exp(-\alpha_0 L)]/\alpha_0$, α_0 is the linear absorption coefficient, and L is the real length of the glass. In order to obtain the parameter β, the parameter $\Delta\psi$ must be deduced. The parameter $\Delta\psi$ can be deduced by the open-aperture Z-scan model, as shown in Fig. 4. The normalized transmittance curve only reflects the information of the third-order optical nonlinear absorption in the open-aperture Z-scan model, and the normalized transmittance curves of the glass exhibit unique peak or valley with respect to the focus ($z=0$) due to the appearance of SA and RSA simultaneously in our experiment. The parameter $\Delta\psi$ is easily extracted from the height or depth of the unique peak ΔT_{p} or valley ΔT_{v} by the following Eq. (3) [46]:

$$\Delta T_{\text{p or v}} = 1 - \frac{\ln(1+\Delta\psi)}{\Delta\psi} \tag{3}$$

where $\Delta T_{\text{p}} = T_{\text{p}} - 1$ or $\Delta T_{\text{v}} = 1 - T_{\text{v}}$, T_{p} and T_{v} represent the height and depth in the normalized transmittance curves of the

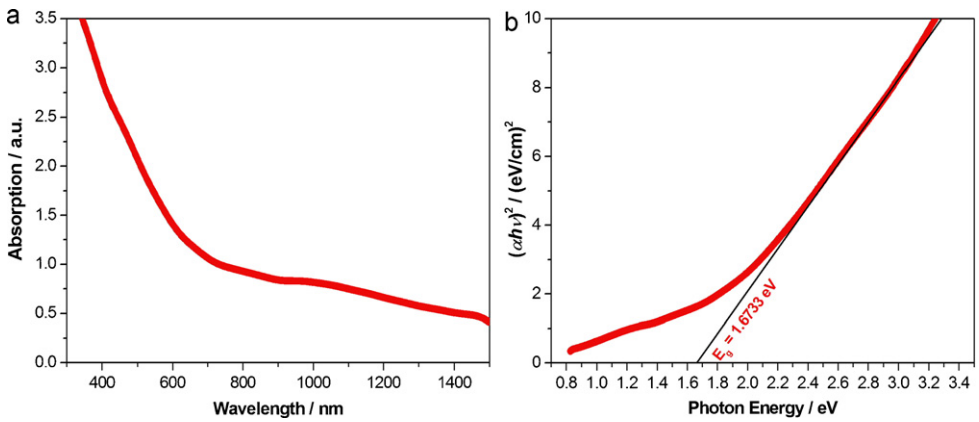

Fig. 4. Optical absorption spectrum: (a) optical absorption spectrum and (b) the spectrum plotted as $[(\alpha h\nu)]^2$ vs. the photon energy ($h\nu$). The solid line is fitting curve to estimate the energy gap E_g.

Table 1
The detailed parameters of the glass in the open-aperture *Z*-scan model.

[a]	$\Delta T_{p\,or\,v}$	$\Delta\psi$	I_0^{OA} ($\times 10^{13}$ W/m^2)	L_{eff} ($\times 10^{-4}$ m)	β ($\times 10^{-9}$ m/W)
I	0.11	0.25	0.78	1.62	0.39
II	0.75	10.4	1.11	1.62	11.6

[a] I and II represent saturable absorption and reverse saturable absorption, respectively.

open-aperture *Z*-scan model, respectively. At last, the detailed parameters are shown in Table 1.

The quantum size effects could be the main cause of the transformation from SA to RSA in the glass. It is well known that an important parameter of semiconductor materials is the energy gap, which separates the conduction band from the valence band. Fig. 6 represents the schematic diagrams of photodynamic for the bulk and nanocrystals in semiconductor materials. One can observe in Fig. 6(a) that this energy gap is a fixed value that is only prescribed by the material's identity in the bulk semiconductor materials. In Fig. 6(a), CB and VB represent the conduction band and valence band, respectively. *E* represents the energy gap. It is the energy difference between the top of the valence band (VB) and the bottom of the conduction band (CB), and the electron in the conduction band (CB) has continuous values of energy. However, when the semiconductor dimensions become comparable to or smaller than the natural length scale of the electron-hole pair, this situation is going to change. The energy gap becomes tunable with the particle size leading to the atomic-like optical behavior instead of bulk bands structure [47]. This phenomenon is known as the quantum size effects. In our experiment, the size of Bi_2S_3 nanocrystals ranges from several to over twenty nanometers, which is smaller than its Bohr radius reported [38]. As a result of the quantum size effects, the energy bands become discrete. The transformation will occur between discrete states arising from the upper states of the valence band (VB) and the lowest energy discrete states arising from the bottom of the conduction band (CB). Also, a number of nearby states available at slightly different energies in the bulk are compressed by the quantum size effects into a single energy level in a quantum dot with the decrease of the particle size. Thus the density of states is increased tremendously, and the energy of the band gap absorption is also increased. As a result, saturable absorption (SA) should be more obvious due to the more transformations from ground state to excited state, which is observed in Fig. 6(b). In addition, the relaxation time in the nanocrystals could be on the subpicosecond to picosecond time scale or longer. One can also observe in Fig. 6(b) that the effective relaxation time of Bi_2S_3 nanocrystals is given by $1/\tau = 1/\tau_{intra} + 1/\tau_{inter} + 1/\tau_{trap}$, where τ_{intra} is the intraband relaxation time, τ_{inter} is the interband relaxation time, and τ_{trap} is the trapping time by surface or defect states. Reverse saturable absorption (RSA) could be mainly derived from the interband transitions among excited states. The small size, narrow distribution, and high dispersion of Bi_2S_3 nanocrystals will lead to the obvious quantum

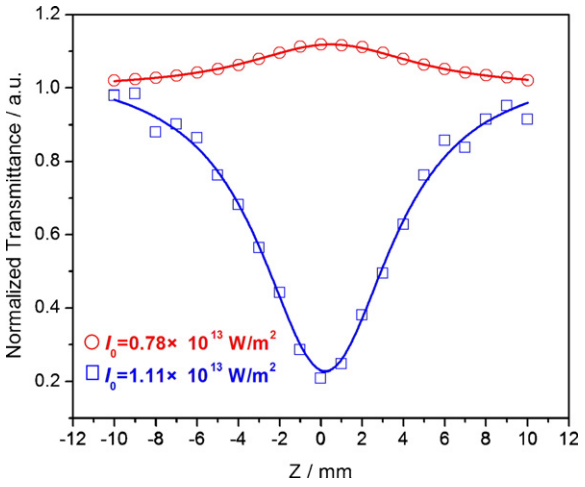

Fig. 5. Open-aperture Z-scan curves of the glass in different input light intensities at 770 nm. I_0 is on-axis peak intensity at focus.

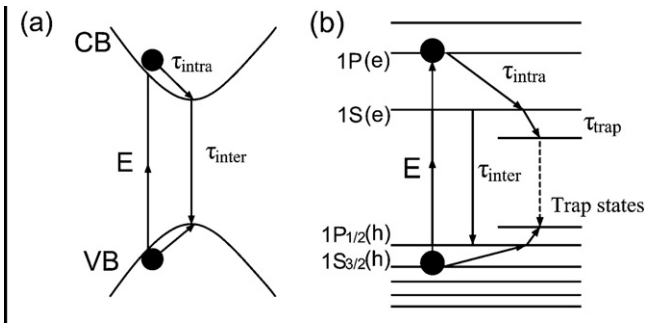

Fig. 6. Schematic illustration of photodynamic in semiconductor materials (a) bulk and (b) nanocrystals.

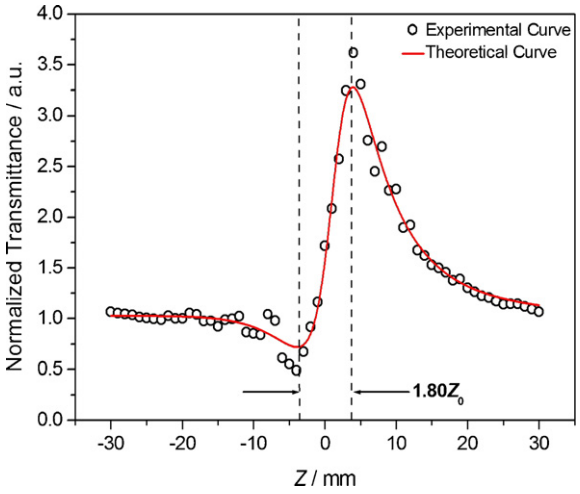

Fig. 7. Closed-aperture Z-scan curve of the glass at 770 nm.

size effects in the glass, which will contribute to the change of the third-order optical nonlinear absorption due to the transitions among these discrete states in the glass.

Besides the quantum size effects, the free-carrier effects, the resonant nonlinear-optical process, the nonlinear scattering, and the thermal effects could also influence the optical nonlinear absorption of the glass in this paper. Generally, the nonlinearities based on the free carrier effects are significant for laser pulses of picosecond (ps) pulses duration [48] and longer [49], which is far greater than that of the laser pulses of femtosecond (fs) pulses duration in this paper. Pejova et al. [50] also reported that the calculated relaxation time of photoexcited charge carriers of Bi_2S_3 is 1.58 ms, which is far greater than the laser pulses of femtosecond pulses duration (~200 fs) in our experiment. Moreover, the input light intensity is also lower in our experiment. Thus the influences of the free carrier effects and the nonlinear scattering are not considered in this paper. In addition, no obvious absorption peaks are observed at a laser frequency of 770 nm, and the nonlinear-optical process should be a non-resonant process in the glass. However, the thermal effects could be more obvious while the *Z*-scan measurement is operated at very high pulse-repetition frequencies. In recent years, the influence of the thermal effects has been widely studied using high repetition rate picosecond (ps) and femtosecond (fs) laser systems in *Z*-scan measurements. Falconieri [51] reported on thermo-optical effects in *Z*-scan measurements using high-repetition-rate lasers and thought that the thermal effects will occur when the laser repetition rate is greater than a few tens of KHz. Mian et al. [52] proposed that a positive deviation of the peak-valley separation from the Kerr value of $1.7z_0$ indicated the presence of thermal contributions. Recently, Chen et al. [53] also drawn the similar conclusion in observing the third-order optical nonlinearities of AgCl doped Bi_2O_3–B_2O_3–SiO_2 ternary glasses. For that the closed-aperture *Z*-scan measurement is operated at 770 nm. Fig. 7 represents the normalized transmittance curve of the closed-aperture *Z*-scan measurement at 770 nm, and the distance between valley and peak at *Z* direction in Fig. 7 is measured in this paper. The calculated value is about $1.80z_0$ ($z_0 = \pi\omega_0^2/\lambda = 4.07$ mm being the Rayleigh range), which has a slight positive deviation from the Kerr value of $1.7z_0$. The result illustrates that the thermal effects should exist in this paper. In addition, the laser repetition rate of 76 MHz, which is greater than a few tens of KHz, further indicates the existence of the thermal effects in this paper. However, the influence of the thermal optical effects is not marked in this paper due to the adjacent value with the Kerr value. One reason could attribute to the high thermal conductivity of the sodium borosilicate glass which promotes the equilibrium temperature in the time between pulses. More researches are needed to explain the influence of the thermal effects in our future work. According to the above-mentioned discussion, the third-order nonlinear optical absorption of the glass should mainly derive from the doping effect of Bi_2S_3 nanocrystals inducing the quantum size effects. Meanwhile, the thermal effects can also not be negligible.

4. Conclusion

The sodium borosilicate glass containing Bi_2S_3 nanocrystals is successfully prepared by employing both sol–gel and atmosphere control methods. These Bi_2S_3 nanocrystals having regular spherical in shape are mounted uniformly in the glass, and the diameters of these spherical nanocrystals range from several to over twenty nanometers. The transformation from saturable absorption (SA) to reverse saturable absorption (RSA) are observed in the glass with the increase of the input light intensities from 0.78×10^{13} and 1.11×10^{13} W/m^2 in the open-aperture *Z*-scan model. The quantum size effects could be the main cause of the transformation from SA to RSA in the glass, and the thermal effects should also be considered. A further confirmation is still needed in the future work about the mechanism of the third-order optical nonlinear absorption in the glass.

Acknowledgments

The work was financially supported by the National Natural Science Foundation of China (Grant nos. 50772075 and 50972107), the Zhejiang Province Natural Science Foundation of China (Grant no. Y4100233), and the Zhejiang Province Key Scientific and Technological Innovations Team of China (Grant no. 2009R50010).

References

[1] W. Denk, J.H. Strickler, W.W. Webb, Science 248 (1990) 73–76.
[2] M. Wittmann, A. Penzkofer, Appl. Phys. B 65 (1997) 49–56.
[3] G.S. He, P.P. Markowicz, T.C. Lin, P.N. Prasad, Nature 415 (2002) 767–770.
[4] G.S. Maciel, N. Rakov, C.B. de Araujo, A.A. Lipovskii, D.K. Tagantsev, Appl. Phys. Lett. 79 (2001) 584–586.
[5] Y.X. Fan, J.L. He, Y.G. Wang, S. Liu, H.T. Wang, Appl. Phys. Lett. 86 (2005) 101103.
[6] G.S. He, K.T. Yong, Q.D. Zheng, Y. Sahoo, A. Baev, A.I. Ryasnyanskiy, P.N. Prasad, Opt. Express 15 (2007) 12818–12833.
[7] E.L. Falcao-Filho, C.A.C. Bosco, G.S. Maciel, L.H. Acioli, C.B. de Araujo, A.A. Lipovskii, D.K. Tagantsev, Phys. Rev. B 69 (2004) 134204.
[8] T. Hasegawa, T. Nagashima, N. Sugimoto, Opt. Commun. 250 (2005) 411–415.
[9] K. Sathiyamoorthy, C. Vijayan, J. Phys. Chem. C 112 (2008) 14336–14342.
[10] T. Kanagasekaran, P. Mythili, P. Srinivasan, A.Y. Nooraldeen, P.K. Palanisamy, R. Gopalakrishnan, Cryst. Growth Des. 8 (2008) 2335–2339.
[11] J. Lv, L. Liang, C.H. Li, X.F. Liu, M.J. Yuan, J.L. Xu, W.D. Zhou, Y.L. Song, H.B. Liu, Y.L. Li, D.B. Zhu, Langmuir 24 (2008) 8297–8302.
[12] M.S. Neo, N. Venkatram, G.S. Li, W.S. Chin, J. Wei, J. Phys. Chem. C 113 (2009) 19055–19060.
[13] U. Gurudas, E. Brooks, D.M. Bubb, S. Heiroth, T. Lippert, A. Wokaun, J. Appl. Phys. 104 (2008) 073107.
[14] H.I. Elim, J. Yang, J.Y. Lee, J. Mi, J. Wei, Appl. Phys. Lett. 88 (2007) 083107.
[15] S.L. Qu, Y.C. Gao, X.W. Jiang, H.D. Zeng, Y.L. Song, J.R. Qiu, C.S. Zhu, K. Hirao, Opt. Commun. 224 (2003) 321–327.
[16] Y.C. Gao, X.R. Zhang, Y.L. Li, H.F. Liu, Y.X. Wang, Q. Chang, W.Y. Jiao, Y.L. Song, Opt. Commun. 251 (2005) 429–433.
[17] Y. Li, M. Takata, A. Nakamura, Phys. Rev. B 57 (1998) 9193–9200.
[18] Y.P. Wang, M.Q. Wang, X. Yao, F.T. Kong, L.Y. Zhang, J. Cryst. Growth 268 (2004) 575–579.
[19] V.I. Klimov, J. Phys. Chem. B 104 (2000) 6112–6123.
[20] H.M. Fan, G.J. You, Y. Li, Z. Zhang, H.R. Tan, Z.X. Shen, S.H. Tang, Y.P. Feng, J. Phys. Chem. C 113 (2009) 9928–9935.
[21] J. He, W. Ji, G.H. Ma, S.H. Tang, E.S.W. Kong, S.Y. Chow, X.H. Zhang, Z.L. Hua, J.L. Shi, J. Phys. Chem. B 109 (2005) 4373–4376.
[22] D. Buso, P. Falcaro, S. Costacurta, M. Guglielmi, A. Martucci, P. Innocenzi, L. Malfatti, V. Bello, G. Mattei, C. Sada, H. Amenitsch, I. Gerdova, A. Haché, Chem. Mater. 17 (2005) 4965–4970.
[23] S.K. Batabyal, L. Tian, N. Venkatram, W. Li, J. Vittal, J. Phys. Chem. C 113 (2009) 15037–15042.
[24] X.H. Wang, Y.M. Du, S. Ding, Q.Q. Wang, G.G. Xiong, M. Xie, X.C. Shen, D.W. Pang, J. Phys. Chem. B 110 (2006) 1566–1570.

[25] X.Y. Yang, W.D. Xiang, X.Y. Zhang, X.J. Liang, H.T. Liu, S.X. Dai, F.F. Chen, J. Mater. Res. 25 (2010) 491–499.
[26] S. Raul, P.K. Nair, V.K. Prashant, Langmuir 14 (1998) 3236–3241.
[27] B.X. Chen, C. Uher, Chem. Mater. 9 (1997) 1655–1658.
[28] W. Tokuda, T. Katoh, A. Yasumori, J. Appl. Phys. 45 (1974) 5908–5909.
[29] B. Miller, A. Heller, Nature 262 (1976) 680–681.
[30] Y. Yu, C.H. Jin, R.H. Wang, Q. Chen, L.M. Peng, J. Phys. Chem. B 109 (2005) 18772–18776.
[31] C.H. Ye, G.W. Meng, Z. Jiang, Y.H. Wang, G.Z. Wang, L.D. Zhang, J. Am. Chem. Soc. 124 (2002) 15180–15181.
[32] G. Xie, Z.P. Qiao, M.H. Zeng, X.M. Chen, S.L. Gao, Cryst. Growth Des. 4 (2004) 513–516.
[33] Z.P. Liu, S. Peng, Q. Xie, Z.K. Hu, Y. Yang, S.Y. Zhang, Y.T. Qian, Adv. Mater. 15 (2003) 936–940.
[34] Q.F. Han, Y. Sun, X. Wang, L. Chen, X.J. Yang, L.D. Lu, J. Alloys Compd. 481 (2009) 520–525.
[35] B. Zhang, X.C. Ye, W.Y. Hou, Y. Zhao, Y. Xie, J. Phys. Chem. B 110 (2006) 8978–8985.
[36] J. Tang, A.P. Alivisatos, Nano Lett. 6 (2006) 2701–2706.
[37] C. Li, G. Shi, Y.L. Song, X.L. Zhang, S.Y. Guang, H.Y. Xu, J. Phys. Chem. Solids 69 (2008) 1829–1834.
[38] B. Pejova, I. Grozdanov, Mater. Chem. Phys. 99 (2006) 39–49.
[39] P.S. Sirimanne, K. Takahashi, N. Sonoyama, T. Sakata, Sol. Energy Mat. Sol. Cells 73 (2002) 175–187.
[40] J. Lu, Q.F. Han, X.J. Yang, L.D. Lu, X. Wang, Mater. Lett. 61 (2007) 2883–2886.
[41] W.H. Li, Mater. Lett. 62 (2008) 243–245.
[42] W.S. Alecer, S.G. Christopher, Q. Wei, A.E. Mostafa, C. Ye, T.M. Valeria, S. Kenneth, Nano Lett. 6 (2006) 1940–1949.
[43] Z.H. Yu, A.H. Megan, E.M.Z. Sara, C. Joaquin, D.K. Todd, S.A. Erik, S. John, ACS Nano 2 (2008) 1179–1188.
[44] T.T. Timothy, S.T. Selvan, L. Zhao, S.J. Gao, Y.Y. Jackie, Chem. Mater. 19 (2007) 3112–3117.
[45] J. Tauc, A. Menth, J. Non-Cryst. Solids 8–10 (1972) 569–585.
[46] M. Sheik-Bahae, A.A. Said, T.H. Wei, D.J. Hagan, E.W. Van Stryland, IEEE J. Quantum Electron. 26 (1990) 760–769.
[47] A.P. Alivisatos, Science 271 (1996) 933–937.
[48] G.P. Banfi, V. Degiorgio, D. Ricard, Adv. Phys. 47 (1998) 447–510.
[49] B.L. Yu, C.S. Zhu, F.X. Gan, X.C. Wu, G.L. Zhang, G.Q. Tang, W.J. Chen, Opt. Mater. 8 (1997) 249–254.
[50] B. Pejova, A. TanuŠevski, I. Grozdanov, J. Solid. State. Chem. 178 (2005) 1786–1798.
[51] M. Falconieri, J. Opt. A: Pure Appl. Opt. 1 (1999) 662–667.
[52] S.M. Mian, S.B. McGee, N. Melikechi, Opt. Commun. 207 (2002) 339–345.
[53] T.F. Xu, F.F. Chen, X. Shen, S.X. Dai, Q.H. Nie, X.S. Wang, Mater. Res. Bull. 45 (2010) 1501–1505.